UNIVERSITY OF BIRMINGHAM
University of Birmingham Research at Birmingham

Wide-angled off-axis achromatic metasurfaces for visible light

Zhang, Shuang; Deng, ZL; Wang, GP

DOI:
10.1364/OE.24.023118

License:
None: All rights reserved

Document Version
Publisher's PDF, also known as Version of record

Citation for published version (Harvard):
Zhang, S, Deng, ZL & Wang, GP 2016, 'Wide-angled off-axis achromatic metasurfaces for visible light', *Optics Express*, vol. 24, no. 20, pp. 23118-23128. https://doi.org/10.1364/OE.24.023118

Link to publication on Research at Birmingham portal

General rights
Unless a licence is specified above, all rights (including copyright and moral rights) in this document are retained by the authors and/or the copyright holders. The express permission of the copyright holder must be obtained for any use of this material other than for purposes permitted by law.

•Users may freely distribute the URL that is used to identify this publication.
•Users may download and/or print one copy of the publication from the University of Birmingham research portal for the purpose of private study or non-commercial research.
•User may use extracts from the document in line with the concept of 'fair dealing' under the Copyright, Designs and Patents Act 1988 (?)
•Users may not further distribute the material nor use it for the purposes of commercial gain.

Where a licence is displayed above, please note the terms and conditions of the licence govern your use of this document.

When citing, please reference the published version.

Take down policy
While the University of Birmingham exercises care and attention in making items available there are rare occasions when an item has been uploaded in error or has been deemed to be commercially or otherwise sensitive.

If you believe that this is the case for this document, please contact UBIRA@lists.bham.ac.uk providing details and we will remove access to the work immediately and investigate.

Download date: 11. May. 2024

Research Article | Vol. 24, No. 20 | 3 Oct 2016 | OPTICS EXPRESS 23118

Optics EXPRESS

Wide-angled off-axis achromatic metasurfaces for visible light

ZI-LAN DENG,[1] SHUANG ZHANG,[2] AND GUO PING WANG[1,*]

[1]*College of Electronic Science and Technology, Guangdong Provincial Key Laboratory of Micro/Nano Optomechatronics Engineering and Key Laboratory of Optoelectronic Devices and Systems of Ministry of Education and Guangdong Province, Shenzhen University, Shenzhen 518060, China*
[2]*School of Physics & Astronomy, University of Birmingham, Birmingham B15 2TT, UK*
[*]*gpwang@szu.edu.cn*

Abstract: We present an approach to build multiwavelength achromatic metasurface that can work in off-axis configuration with an ultra-wide applicable incident angle range for visible light. The metasurface is constructed by combining multiple metallic nano-groove gratings, which support enhanced diffractions for transverse magnetic polarization in an ultrawide incident angle range from 10° to 80° due to the excitations of localized gap plasmon modes at different resonance wavelengths. To achieve the achromatic diffraction, the ratio between the resonance wavelength and the period of each elementary grating is fixed. Incident light at those multiple resonance wavelengths can be efficiently diffracted into the same direction with near-complete suppression of the specular reflection. Based on the similar approach, we also design a wide-angled off-axis achromatic flat lens for focusing light of different wavelengths into the same position. Our findings provide an alternative simple way to design various off-axis achromatic flat optical elements without stringent angle requirement for imaging and display applications.

© 2016 Optical Society of America

OCIS codes: (160.3918) Metamaterials; (250.5403) Plasmonics; (050.1950) Diffraction gratings; (090.1760) Computer holography.

References and links

1. B. C. Kress and P. Meyrueis, *Applied Digital Optics* (Wiley, 2009).
2. N. Yu, P. Genevet, M. A. Kats, F. Aieta, J.-P. Tetienne, F. Capasso, and Z. Gaburro, "Light propagation with phase discontinuities: generalized laws of reflection and refraction," Science **334**(6054), 333–337 (2011).
3. F. Aieta, P. Genevet, N. Yu, M. A. Kats, Z. Gaburro, and F. Capasso, "Out-of-plane reflection and refraction of light by anisotropic optical antenna metasurfaces with phase discontinuities," Nano Lett. **12**(3), 1702–1706 (2012).
4. S. Sun, Q. He, S. Xiao, Q. Xu, X. Li, and L. Zhou, "Gradient-index meta-surfaces as a bridge linking propagating waves and surface waves," Nat. Mater. **11**(5), 426–431 (2012).
5. L. Huang, X. Chen, H. Mühlenbernd, G. Li, B. Bai, Q. Tan, G. Jin, T. Zentgraf, and S. Zhang, "Dispersionless phase discontinuities for controlling light propagation," Nano Lett. **12**(11), 5750–5755 (2012).
6. D. Lin, P. Fan, E. Hasman, and M. L. Brongersma, "Dielectric gradient metasurface optical elements," Science **345**(6194), 298–302 (2014).
7. L. Zhang, J. Hao, M. Qiu, S. Zouhdi, J. K. W. Yang, and C.-W. Qiu, "Anomalous behavior of nearly-entire visible band manipulated with degenerated image dipole array," Nanoscale **6**(21), 12303–12309 (2014).
8. X. Su, C. Ouyang, N. Xu, W. Cao, X. Wei, G. Song, J. Gu, Z. Tian, J. F. O'Hara, J. Han, and W. Zhang, "Active metasurface terahertz deflector with phase discontinuities," Opt. Express **23**(21), 27152–27158 (2015).
9. F. Aieta, P. Genevet, M. A. Kats, N. Yu, R. Blanchard, Z. Gaburro, and F. Capasso, "Aberration-free ultrathin flat lenses and axicons at telecom wavelengths based on plasmonic metasurfaces," Nano Lett. **12**(9), 4932–4936 (2012).
10. M. Khorasaninejad, W. T. Chen, R. C. Devlin, J. Oh, A. Y. Zhu, and F. Capasso, "Metalenses at visible wavelengths: Diffraction-limited focusing and subwavelength resolution imaging," Science **352**(6290), 1190–1194 (2016).
11. X. Chen, L. Huang, H. Mühlenbernd, G. Li, B. Bai, Q. Tan, G. Jin, C.-W. Qiu, S. Zhang, and T. Zentgraf, "Dual-polarity plasmonic metalens for visible light," Nat. Commun. **3**, 1198 (2012).
12. X. Li, S. Xiao, B. Cai, Q. He, T. J. Cui, and L. Zhou, "Flat metasurfaces to focus electromagnetic waves in reflection geometry," Opt. Lett. **37**(23), 4940–4942 (2012).

#273383 http://dx.doi.org/10.1364/OE.24.023118
Journal © 2016 Received 10 Aug 2016; revised 1 Sep 2016; accepted 3 Sep 2016; published 26 Sep 2016

Optics EXPRESS

13. L. Huang, X. Chen, H. Mühlenbernd, H. Zhang, S. Chen, B. Bai, Q. Tan, G. Jin, K.-W. Cheah, C.-W. Qiu, J. Li, T. Zentgraf, and S. Zhang, "Three-dimensional optical holography using a plasmonic metasurface," Nat. Commun. **4**, 2808 (2013).
14. X. Ni, A. V. Kildishev, and V. M. Shalaev, "Metasurface holograms for visible light," Nat. Commun. **4**, 3807 (2013).
15. G. Zheng, H. Mühlenbernd, M. Kenney, G. Li, T. Zentgraf, and S. Zhang, "Metasurface holograms reaching 80% efficiency," Nat. Nanotechnol. **10**(4), 308–312 (2015).
16. Y.-H. Chen, L. Huang, L. Gan, and Z.-Y. Li, "Wavefront shaping of infrared light through a subwavelength hole," Light Sci. Appl. **1**(8), e26 (2012).
17. K. E. Chong, L. Wang, I. Staude, A. R. James, J. Dominguez, S. Liu, G. S. Subramania, M. Decker, D. N. Neshev, I. Brener, and Y. S. Kivshar, "Efficient polarization-insensitive complex wavefront control using huygens' metasurfaces based on dielectric resonant meta-atoms," ACS Photonics **3**(4), 514–519 (2016).
18. D. Wen, F. Yue, G. Li, G. Zheng, K. Chan, S. Chen, M. Chen, K. F. Li, P. W. H. Wong, K. W. Cheah, E. Y. Pun, S. Zhang, and X. Chen, "Helicity multiplexed broadband metasurface holograms," Nat. Commun. **6**, 8241 (2015).
19. A. Arbabi, Y. Horie, M. Bagheri, and A. Faraon, "Dielectric metasurfaces for complete control of phase and polarization with subwavelength spatial resolution and high transmission," Nat. Nanotechnol. **10**(11), 937–943 (2015).
20. D. Wen, S. Chen, F. Yue, K. Chan, M. Chen, M. Ardron, K. F. Li, P. W. H. Wong, K. W. Cheah, E. Y. B. Pun, G. Li, S. Zhang, and X. Chen, "Metasurface device with helicity-dependent functionality," Adv. Opt. Mater. **4**(2), 321–327 (2016).
21. I. Dolev, I. Epstein, and A. Arie, "Surface-plasmon holographic beam shaping," Phys. Rev. Lett. **109**(20), 203903 (2012).
22. P. Genevet, J. Lin, M. A. Kats, and F. Capasso, "Holographic detection of the orbital angular momentum of light with plasmonic photodiodes," Nat. Commun. **3**, 1278 (2012).
23. J. Lin, P. Genevet, M. A. Kats, N. Antoniou, and F. Capasso, "Nanostructured holograms for broadband manipulation of vector beams," Nano Lett. **13**(9), 4269–4274 (2013).
24. Z.-L. Deng, S. Zhang, and G. P. Wang, "A facile grating approach towards broadband, wide-angle and high-efficiency holographic metasurfaces," Nanoscale **8**(3), 1588–1594 (2016).
25. B. G. Cai, Y. B. Li, W. X. Jiang, Q. Cheng, and T. J. Cui, "Generation of spatial Bessel beams using holographic metasurface," Opt. Express **23**(6), 7593–7601 (2015).
26. P. Genevet and F. Capasso, "Holographic optical metasurfaces: a review of current progress," Rep. Prog. Phys. **78**(2), 024401 (2015).
27. J. Cheng, D. Ansari-Oghol-Beig, and H. Mosallaei, "Wave manipulation with designer dielectric metasurfaces," Opt. Lett. **39**(21), 6285–6288 (2014).
28. M. M. Salary, M. Nazari, and H. Mosallaei, "Robust technique for computation of scattering and absorption of light by array of nanowires on layered substrate," J. Opt. Soc. Am. B **32**(12), 2448–2461 (2015).
29. T. Yatooshi, A. Ishikawa, and K. Tsuruta, "Terahertz wavefront control by tunable metasurface made of graphene ribbons," Appl. Phys. Lett. **107**(5), 053105 (2015).
30. T. Li, S. Wang, X.-L. Zhang, Z.-L. Deng, Z. H. Hang, H.-B. Sun, and G. P. Wang, "Non-uniform annular rings-based metasurfaces for high-efficient and polarization-independent focusing," Appl. Phys. Lett. **107**(25), 251107 (2015).
31. F. Zhou, W. Cao, B. Dong, T. Reissman, W. Zhang, and C. Sun, "Additive manufacturing of a 3D terahertz gradient-refractive index lens," Adv. Opt. Mater. **4**(7), 1034–1040 (2016).
32. F. Aieta, M. A. Kats, P. Genevet, and F. Capasso, "Multiwavelength achromatic metasurfaces by dispersive phase compensation," Science **347**(6228), 1342–1345 (2015).
33. M. Khorasaninejad, F. Aieta, P. Kanhaiya, M. A. Kats, P. Genevet, D. Rousso, and F. Capasso, "Achromatic Metasurface Lens at Telecommunication Wavelengths," Nano Lett. **15**(8), 5358–5362 (2015).
34. Y. Li, X. Li, M. Pu, Z. Zhao, X. Ma, Y. Wang, and X. Luo, "Achromatic flat optical components via compensation between structure and material dispersions," Sci. Rep. **6**, 19885 (2016).
35. Z. Zhao, M. Pu, H. Gao, J. Jin, X. Li, X. Ma, Y. Wang, P. Gao, and X. Luo, "Multispectral optical metasurfaces enabled by achromatic phase transition," Sci. Rep. **5**, 15781 (2015).
36. J. Cheng and H. Mosallaei, "Truly achromatic optical metasurfaces: a filter circuit theory-based design," J. Opt. Soc. Am. B **32**(10), 2115–2121 (2015).
37. Y.-K. R. Wu, A. E. Hollowell, C. Zhang, and L. J. Guo, "Angle-insensitive structural colours based on metallic nanocavities and coloured pixels beyond the diffraction limit," Sci. Rep. **3**, 1194 (2013).
38. D. L. Sounas and A. Alù, "Color separation through spectrally-selective optical funneling," ACS Photonics **3**(4), 620–626 (2016).
39. P. B. Johnson and R. W. Christy, "Optical constants of the noble metals," Phys. Rev. B **6**(12), 4370–4379 (1972).
40. W.-H. Lee, "Binary computer-generated holograms," Appl. Opt. **18**(21), 3661–3669 (1979).
41. G. P. Wang, T. Sugiura, and S. Kawata, "Holography with surface-plasmon-coupled waveguide modes," Appl. Opt. **40**(22), 3649–3653 (2001).

Optics EXPRESS

1. Introduction

Optical elements without stringent incident angle requirement are highly desired in practical imaging and display systems, such as the full-angle photographing and panoramic viewing system. There are several conventional ways for realizing wide-angled achromatic imaging systems, such as introduction of achromatic doublet or achromatic triplet, and multiple order diffractive lenses [1]. Those methods, however, require cascaded multiple thick components and are therefore bulky and cumbersome.

To overcome the disadvantage of traditional optical elements, much attention has been paid to ultra-thin flat structures, known as metasurfaces, which consist of two-dimensional (2D) array of subwavelength structures [2–30] and exhibit various functionalities including wave deflection [2–8], focusing [9–12, 31], holographic display [13–17], polarization multiplexing [18–20], and beam-shaping [21–25]. Recently, the achromatization was also demonstrated in flat metasurface structures, such as the suitably designed metasurface composed of coupled rectangular dielectric resonators (RDRs) [32, 33], metallic hole and slit arrays [34, 35], circuit theory-based metasurfaces [36], and so on, which show great potential for high-quality imaging with only a lightweight thin structure. Most of the previous approaches to achieve achromatization, if not all, need complex design and are mainly for on-axis applications that require only a narrow incident angle range [Fig. 1(a)]. Although on-axis optical components are widely used in typical optical systems, the off-axis optical components with large incident angle are also highly desired in some specific imaging and projection systems, such as off-axial Three-mirror Anastigmat, unobstructed spatial observing telescope and so on.

In this paper, we present an alternative facile approach to design multiwavelength achromatic metasurfaces that work for off-axis configuration with an ultrawide incident angle range [Fig. 1(b)]. The metasurface is a combination of multiple sets of metallic nano-groove gratings, each of which has a unique period and groove height to work for a particular wavelength [Fig. 1(c)]. It has been shown previously that the wide nano-groove metasurface can deflect light with very high diffraction efficiency and near-completely suppress the unwanted specular reflection in a broadband, wide-angle range [24]. Although the previous proposed metasurface works for broadband, the chromatic behavior still exists due to the dispersion phenomenon of the grating. In order to design achromatic metasurface with wide-angle performance, here, we choose multiple narrow nano-groove gratings with fixed ratio between resonance wavelength and grating period as elementary gratings, and then combine them to achieve achromatic diffraction and focusing. Each narrow groove grating has enhanced diffraction efficiency in a narrow band due to excitation of localized plasmon mode in the grooves. As the localized plasmon mode is independent of incident angle of the illuminating light, the enhanced diffraction efficiency exists for a very wide angular range. Besides the nano-groove structure, the concept developed here can be extend to other localized resonator arrays such as localized dielectric resonators, graphene ribbons and so on. Note that, the localized resonances are also recently used to wide-angled color display devices [37, 38]. The narrow band of each elementary grating also decrease the crosstalk between grooves of different depths when multiple gratings are combined. It is demonstrated that, the combined nano-groove metasurface can diffract the incident light to the same direction for different wavelengths, even if the incident angle is varied in an ultrawide range. By modulating the elementary grating with a quadratic phase profile, we also obtain a wide-angled achromatic focusing metasurface, which can focus the incident light of different wavelengths into the same position.

Optics EXPRESS

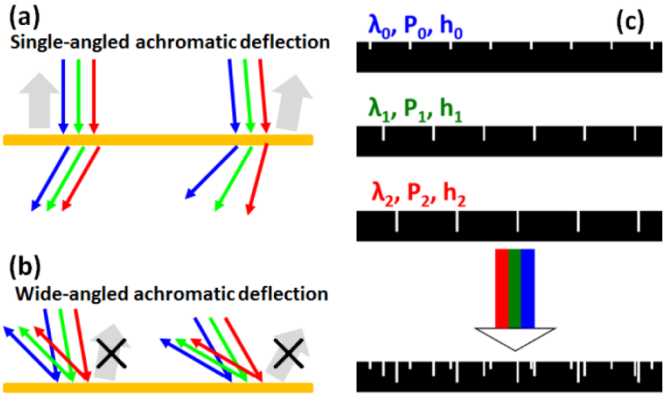

Fig. 1. (a, b) Schematic of the (a) on-axis narrow-angled and (b) off-axis wide-angled achromatic deflection by a metasurface (orange). (c) Schematic of formation of the ultrawide-angled achromatic metasurface by combining multiple metallic nano-groove gratings with different periods (p_0, p_1, and p_2) and groove heights (h_0, h_1, and h_2). The elementary gratings support the near-total diffraction in the −1st order at different wavelengths (λ_0, λ_1, and λ_2) due to the excitation of the localized gap plasmon mode in the nano-grooves with different heights (h_0, h_1, and h_2).

2. Results and Discussion

2.1. The diffraction properties of the single groove grating

For a metallic nano-groove grating, the relation between the reflection angle of the −1st diffraction order θ_r and incident angle θ_0 is determined by,

$$\sin\theta_r = \sin\theta_0 - \lambda / p, \tag{1}$$

where, λ and p are the wavelength of incident light and period of the grating, respectively. From Eq. (1) we see that, the reflection angle is dependent on the wavelength of light, which is the well-known chromatic dispersion existing in a common grating. If λ/p is fixed, however, the reflection angle will be fixed for a given incident angle θ_0. Therefore, in order to obtain the same diffraction angle for multiple wavelengths (λ_0, λ_1, and λ_2), one can choose multiple gratings (g_0, g_1, and g_2) with fixed wavelength/period ratio ($\lambda_0/p_0 = \lambda_1/p_1 = \lambda_2/p_2$). To ensure the enhanced diffraction in the −1st order, the groove heights (h_0, h_1, and h_2) of the multiple gratings should be suitably chosen so that the lights with wavelengths λ_0, λ_1, and λ_2 just excite the corresponding cavity modes in the nano-grooves, respectively. The cavity mode in the metallic groove originates from the Fabry-Perot resonance of the fundamental waveguide mode in a truncated metal-insulator-metal (MIM) structure. In visible frequency range, the fundamental waveguide mode in MIM can be seen as the gap plasmon mode whose field is localized in the gap and metallic surface area, especially when the gap width is very narrow (<200nm). By combining those elementary gratings together, we could hence expect to obtain an achromatic metasurface as schematically illustrated in Fig. 1(c).

Optics EXPRESS

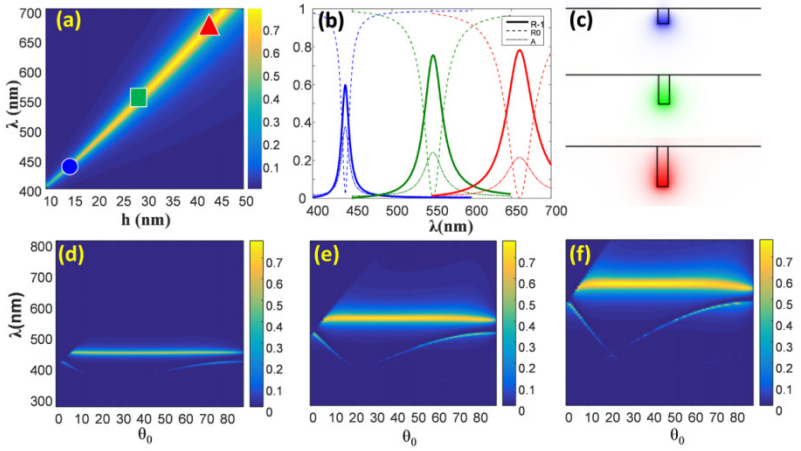

Fig. 2. (a) The −1st diffraction efficiency (shown by color bar) of an elementary grating for varying groove height *h* and incident wavelength λ, when a TM polarized plane wave incidents the structure with angle 45°. The ratio of wavelength and period of the grating is fixed as λ/p = 1.1. (b) The −1st (solid), 0th (dashed) diffraction efficiencies (R_{-1}, R_0) and the absorption A (dot-dashed) for three elementary gratings (g_0, g_1, and g_2), whose geometry parameters are indicated by blue circle, green square, and red triangle, respectively, in (a). (c) The field patterns ($|H_z|^2$) at the peak position of R_{-1} of the three elementary gratings. (d-f) The −1st diffraction efficiency (shown by color bar) of the three elementary gratings, respectively, as a function of incident wavelength and incident angle.

To determine the groove height of each elementary grating, we calculated the dependence of the −1st diffraction efficiency (denoted as R_{-1}) of the grating illuminated by transverse magnetic (TM) polarized light at incident angle 45° upon groove height *h* and incident wavelength λ [Fig. 2(a)] by finite element method (FEM), which is implemented by a commercial software COMSOL. In the calculation, silver is chosen as the metal material, with permittivity obtained by fitting the experimental data [39] to the Drude model, and the metallic groove width is fixed as *w* = 10nm. The ratio between the incident wavelength and the grating period, are fixed in the calculations at λ/p = 1.1. Note that, the value of λ/p should be chosen in the range $2/3<\lambda/p<2$ so that the localized plasmon mode resonance locates within the area bounded by the −2nd, −1st and 1st Rayleigh Anomalies. Actually, the applicable angle range is the largest at λ/p = 1 [24]. We choose λ/p = 1.1, which is a little larger than 1 because the resonance peak for λ/p = 1.1 not only extends a large applicable angle range, but also exhibits the most flat profile. Figure 2(a) shows that the spectral peak wavelength of R_{-1} is linear to the groove height of the grating. When the groove height is varied from 10nm to 50nm, the wavelength of peak diffraction efficiency spans the entire visible wavelengths ranging from 400nm to 700nm. Hence we can select three sets of gratings - g_0: p_0 = 400nm, h_0 = 15nm; g_1: p_1 = 500, h_1 = 29nm; and g_2: p_2 = 600nm, h_2 = 42nm, corresponding to wavelengths in the blue (λ = 440nm), green (550nm), and red (660nm) color regions as indicated by the blue circle, green square and red triangle, respectively, in Fig. 2(a). The diffraction efficiencies of the 0th (R_0) and −1st (R_{-1}) orders as well as the absorption (A) of the three gratings are shown in Fig. 2(b). It is clear that the −1st diffraction efficiencies (solid curves) of the three gratings exhibit resonant peaks at 440nm, 550nm and 660nm, respectively. In contrast, the unwanted 0th diffraction efficiencies (dashed curves) approach zero at the three resonant wavelengths, indicating a nearly complete suppression of the specular reflections. The absorption (represented by dot-dashed curves) also exhibits peak values at the resonant wavelengths, and the shorter the resonant wavelength, the stronger the absorption due to the stronger intrinsic absorption of metal at shorter wavelength. Nevertheless, the −1st diffraction efficiencies can still reach high values larger than 0.6.

Optics EXPRESS

To shed light on the origin of the enhanced diffraction efficiency of the −1st order, we plot the field patterns ($|H_z|^2$) at the R_{-1} peak wavelengths of the three gratings in Fig. 2(c). The fields are mainly localized inside the groove regions of the gratings with a small part penetrating into the metal, which are typical field profiles of the localized plasmon modes, indicating that the strong diffraction efficiencies of R_{-1} are indeed caused by the excitations of the localized plasmon modes. Because the localized plasmon modes are independent of the incident angles of the illuminating light, the enhanced diffraction efficiencies should exist for a broad range of incident angles. Figures 2(d)-2(f) plot the R_{-1} as a function of the incident angle θ_0 and wavelength λ of the illuminating light for the three gratings, respectively. The peak wavelength of R_{-1} for all the three gratings remains constant for almost all incident angles. The peak value is the highest at incident angle of 45°, and it gradually decrease when θ_0 approaches 0° or 90°. As a whole, the diffraction peak exists for an ultrawide angle range of 10° to 80°, which promises the wide-angle performance of the achromatic metasurface.

2.2. The coupling effect of different nano-grooves in the compound grating

Before combing the elementary narrow groove gratings into achromatic metasurfaces, let's first study the coupling effect of the grooves with different heights for varying spacings between adjacent grooves. Figure 3 shows diffraction efficiencies of the compound grating, of which there are three grooves with h_1 = 15nm, h_2 = 29nm, and h_3 = 42nm, respectively, in each period. For the compound grating with p = 400nm [Fig. 3(a)], we observe the diffraction efficiency variation versus spacing at wavelength of 440nm, which is the resonance wavelength of the individual groove with h_1 = 15nm. The −1st diffraction efficiency sustains high values when spacing is greater than a critical value of about s_0 = 7nm, while below this critical value, it decreases dramatically. It is because, for large spacing ($s>s_0$), the coupling between grooves is very weak, the resonance is still mainly determined by the individual groove, as the field is mainly localized in the individual groove [right inset of Fig. 3(a)]; for small spacing ($s<s_0$), however, the inter-groove coupling is very strong and the resonance wavelength will be influenced by all the grooves [left inset of Fig. 3(a)], as a result, the resonance peak of R_{-1} shifts to longer wavelength [Fig. 4(a)]. For the compound grating with p = 500nm at working wavelength λ = 550nm [Fig. 3(b)], the critical spacing is slightly larger (s_0 = 12nm), the field is mainly localized in the h_2 groove [right inset of Fig. 3(b)] when $s>s_0$, while it extends to all the three grooves [left inset of Fig. 3(b)] due to strong coupling when $s<s_0$. For the compound grating with p = 600nm at working wavelength λ = 660nm, the critical spacing is even larger (s_0 = 30nm), the field is localized in the h_3 groove [right inset of Fig. 3(c)] above the critical spacing, while it extends to the h_2 and h_3 grooves below the critical spacing.

Optics EXPRESS

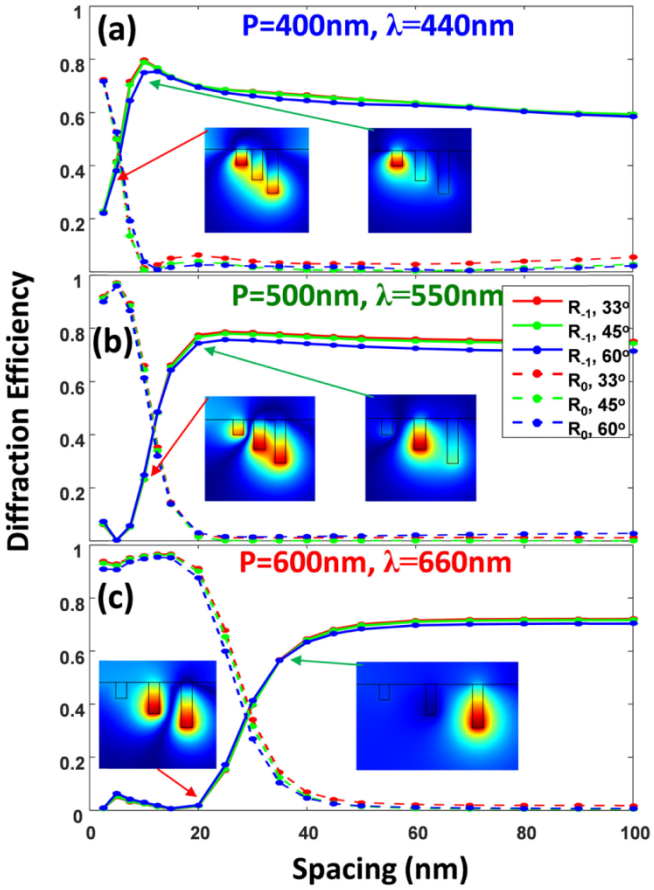

Fig. 3. The diffraction efficiencies (R_{-1}: solid, R_0: dashed) of the compound grating with three different nano-grooves in each unit cell with varying spacings between adjacent nano-grooves. The grating period and incident wavelength are (a) p = 400nm, λ = 440nm; (b) p = 500nm, λ = 550nm; (c) p = 600nm, λ = 660nm, respectively. Different incident angles: 33° (red), 45° (green), and 60° (blue) are applied in the calculation. The insets show the field patterns ($|H_z|^2$) of the grooves at strong coupling region (left), and weak coupling region (right), respectively.

From the −1st reflection spectra of the compound gratings in Fig. 4, we can clearly see that, when the groove spacing is larger than the critical spacing, the resonance peek stays in the same wavelength position, while the peak shift dramatically to longer wavelength as long as the spacing is smaller than the critical spacing. And the longer the wavelength, the larger the critical spacing, which can be attributed to the positive correlation between the effective coupling length and the working wavelength.

Optics EXPRESS

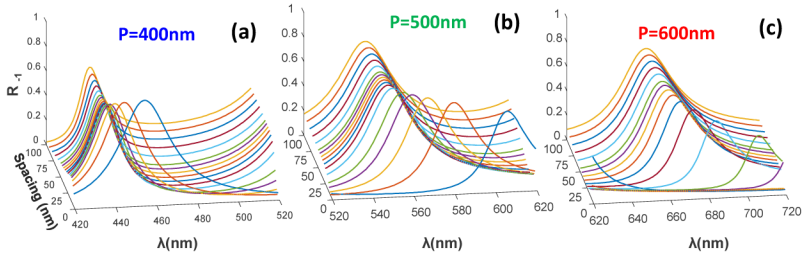

Fig. 4. The −1st reflection spectra for the compound grating for (a) p = 400nm, (b) p = 500nm, and (c) p = 600nm, respectively, with three different nano-grooves (h_1 = 15nm, h_2 = 29nm, h_3 = 42nm) in each unit cell for different spacings between adjacent nano-grooves.

2.3 The achromatic diffraction metasurface by combining multiple periodic gratings

By combining the three sets of the elementary gratings (g_0, g_1, and g_2), we can construct an achromatic metasurface as shown by the bottom panel in Fig. 1(c). The resonance wavelengths of the three gratings are 440nm, 550nm, and 660nm, which correspond to blue, green and red colors, respectively. Figures 5(d)-5(l) show the FEM simulations of the combined metasurface illuminated by a Gaussian beam of blue (440nm), green (550nm), and red (660nm) color, respectively. When a Gaussian beam illuminates on the metasurface from the left side with an incident angle of 45°, the beam is reflected to the left side (negative reflection), whereas the specular reflection (to the right side) is completely suppressed. For all the three different wavelengths, the directions of the negative reflection remain the same [Figs. 5(d)-5(f)]. It is because when a Gaussian Beam with a specific wavelength illuminate the metasurface, only the gap plasmon mode in the nano-grooves that resonate at this wavelength is excited, whereas other nano-grooves do not respond to this wavelength due to large separation of the resonance frequencies and the weak coupling between localized resonances of the nano-grooves [see Fig. 2(b) and Fig. 3]. For comparison, we also plot the case for an ordinary metallic grating illuminated by the same Gaussian beams as shown in Figs. 5(a)-5(c). The diffraction directions are apparently different for different wavelengths, which is the well-known chromatic characteristic of a conventional grating.

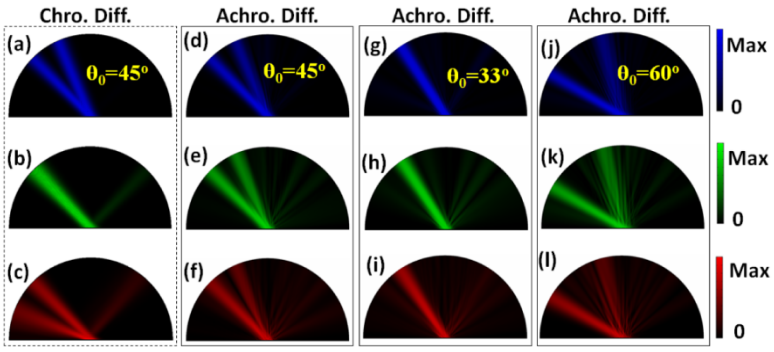

Fig. 5. The field patterns ($|H_z|^2$) of (a-c) the common chromatic diffraction grating and (d-l) the achromatic diffraction metasurface, respectively. The structure is illuminated by a Gaussian beam with (upper row) blue (440nm), (middle row) green (550nm), and (lower row) red (660nm) color, respectively. The incident angle is (a-f) 45°, (g-i) 33°, (j-l) 60°, respectively.

The achromatic diffraction can exist for an ultrawide range of incident angles, as verified by the simulation for other incident angles as shown in Figs. 5(g)-5(l). When the Gaussian beam illuminates the metasurface at θ_0 = 33° [Figs. 5(g)-5(i)], the beam is reflected back along its original path, because this particular incident angle satisfies the Littrow mount condition. Again, this works for all three wavelengths. The achromatic diffractions of the

Optics EXPRESS

metasurface also exist for incident angle of 60° for the three wavelengths as shown in Figs. 5(j)-5(l). Incident beams are routed into the −1st diffraction order with the same diffraction angle (13.5°), while the specular reflections are completely suppressed. Therefore, the achromatic diffractions are indeed applicable for a wide incident angle range, which is highly desired for practical operations. The conversion efficiency of the combined achromatic diffraction metasurface is near 0.5 for 440nm and 550nm, while it only reaches about 0.35 for 660nm [see Table 1]. It can be explained by the fact that, the critical spacing for λ = 660nm [Fig. 3(c)] is much larger than that for λ = 440nm and 550nm [Figs. 3(a) and (b)], respectively. The combined metasurface may contain some units with small groove spacings that are larger than the critical spacing for 440nm and 550nm, but smaller than the critical spacing for 660nm, as a result, the total conversion efficiencies at λ = 660nm are significantly reduced.

Table 1. Conversion efficiency of the achromatic diffraction metasurface.

Angle / Wavelength	33°	45°	60°
440nm	0.531	0.539	0.491
550nm	0.511	0.536	0.508
660nm	0.347	0.360	0.359

2.4 The achromatic focusing metasurface by combining multiple modulated gratings

The wide-angle achromatic diffraction of the off-axis metasurface can be extended to the achromatic shaping of arbitrary wavefront with wide applicable incident angle range. Based on the relation between the phase and grating period [24], we can modulate the periods of each of the three sets of elementary gratings for achieving a desired phase profile by designing the height profile $h_{x,y}$ of the grating with binary hologram techniques [40, 41],

$$h_{x,y} = \frac{h}{2}\left(1+\mathrm{sgn}\left(\cos\left(2\pi x / p+\phi(x,y)\right)\right)\right), \tag{2}$$

where, h is the groove height; p is the central period of the grating, the actual period of grating is modulated by $\phi(x,y)$, which is the phase profile of the desired wavefront. Note that, based on just a simple one-dimensional (1D) grating with profile $2\pi x/p$, we can modulate an arbitrary wavefront with 2D phase distribution $\phi(x,y)$. Then we can combine the modulated gratings to form an achromatic metasurface for shaping the wavefront for all three wavelengths.

As a simple example, we now demonstrate the wide-angle achromatic 1D lens by the above approach. To obtain the focusing in the off-axis direction (−1st diffraction) with angle θ_r, the phase profile in the metasurface plane should be

$$\phi(x,y) = k_i\left(\sqrt{f^2\cos^2\theta_r+\left(f\sin\theta_r+x\right)^2}-f\right)-k_i x\sin\theta_r, \tag{3}$$

where f is the focus length, k_i is the wavevecor of the incident wave, and i = 0, 1, 2 corresponds to the three different colors. Note that, if the focus length satisfies the limit $x/f \ll 1$, the phase profile can be simplified as,

$$\phi(x,y) = k_i f\left(1+\frac{x}{f}\sin\theta_r+\frac{x^2}{2f^2}-1\right)-k_i x\sin\theta_r = \frac{k_i x^2}{2f}, \tag{4}$$

which is the same as the quadratic phase profile of an on-axis focusing lens.

Optics EXPRESS

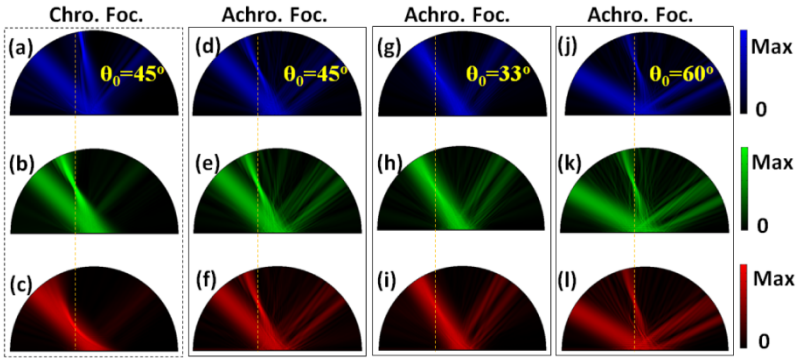

Fig. 6. The field patterns ($|Hz|^2$) of (a-c) the common off-axis lens and (d-l) the achromatic focusing metasurface, respectively. The structure is illuminated by a Gaussian beam with (upper row) blue (440nm), (middle row) green (550nm), and (lower row) red (660nm) color, respectively. The incident angle is (a-f) 45°, (g-i) 33°, (j-l) 60°, respectively.

Table 2. Conversion efficiency of the achromatic focusing metasurface.

Angle / Wavelength	33°	45°	60°
440nm	0.477	0.401	0.286
550nm	0.552	0.489	0.335
660nm	0.420	0.382	0.260

Due to the different wavevector for each color, this design leads to a different gradient period profile for each of the elementary grating. By carefully combining those three gradient gratings in the same way as shown in Fig. 1(c), we can obtain the metasurface as an achromatic flat lens for focusing. Figures 6(d)-6(f) show the field patterns ($|H_z|^2$) when the focusing metasurface ($f = 20\mu m$) is obliquely ($\theta_0 = 45°$) illuminated by a Gaussian beam with different wavelengths. It is observed that the reflection waves are primarily redirected into the −1st diffraction order, and are focused at approximately the same position for different colors as indicated by the dashed line in Figs. 6(d)-6(f) for all the three wavelengths. In comparison, Figs. 6(a)-6(c) show the corresponding field patterns for an ordinary off-axis lens constructed by a single gradient grating. The incident Gaussian beam can also be focused, but the focusing point is obviously different for different wavelengths due to the intrinsic chromatic characteristic of the single grating. Therefore, the combined metasurface can indeed work as a multiwavelength achromatic flat lens. To demonstrate the wide-angle performance of the focusing metasurface, we also simulate the cases for other incident angles of the Gaussian beam as shown in Figs. 6(g)-6(l). When the Gaussian beam illuminates the metasurface with incident angle 33° [Figs. 6(g)-6(i)], the beam is primarily reflected back along its original incident path, and focused in the same point (−10.7um, 16.8um) even if the color of the incident light is different. Similarly, when the incident angle is 60° [Fig. 6(j)-6(l)], majority of light can also be focused at a same point (−4.4um, 19.0um) for all the three wavelengths. From the intensity profile at the focal plane of the focusing metasurface as shown in Fig. 7, we can see that, the focusing beam width (1μm) is significantly smaller than incident beam width (5μm), and the focusing positions of the three wavelengths with blue, green and red colors, respectively, are indeed the same, which further proves the achromatic property of the combined metasurface. The peak value and the conversion efficiency [see Table 2] for 660nm is smaller than those for the other two short wavelengths, which is also due to the small groove spacings of the combined metasurface that is larger than the critical spacing for 440nm and 550nm, but smaller than that for 660nm [see Fig. 3(a)-3(c)].

Optics EXPRESS

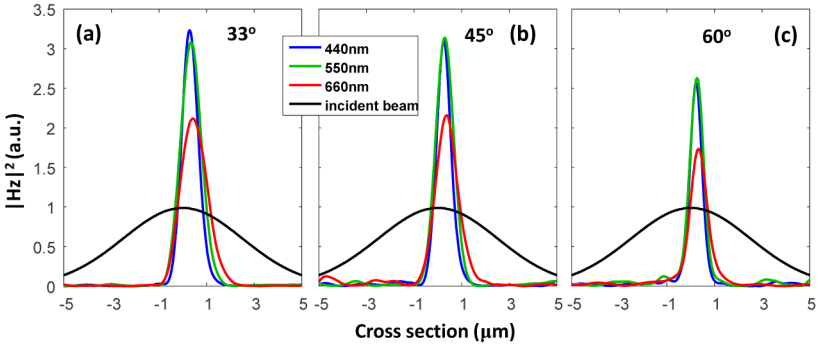

Fig. 7. Cross section cuts of $|H_z|^2$ for wavelength of 440nm (blue), 550nm (green), and 660nm (red), respectively, in the focal plane of the off-axis achromatic focusing metasurface with different incident angles (a) 33°, (b) 45°, and (c) 60°, respectively. The black curves represent the corresponding intensity profile of the incident Gaussian beam.

3. Summary

In summary, we introduce a type of off-axis multiwavelengths achromatic metasurfaces with wide-angle performance. The metasurface is constructed by integrating multiple metallic gratings with different subwavelength grooves in a single surface. The groove height of each elementary grating determines the corresponding resonance wavelength for enhanced diffraction, and the ratio between the resonance wavelength and grating period is fixed to achieve the achromatic operations. Such metasurfaces are utilized to demonstrate achromatic diffraction and focusing for visible light. The superior performance of the achromatic metasurfaces proposed here may pave the way towards practical applications in imaging and display systems.

Funding

National Natural Science Foundation of China (NSFC) (11604217, 11274247, 11574218, 11504243, 61501302); Natural Science Foundation of Guangdong Province, China (2015A030310400, 2016A030313042); China Postdoctoral Science Foundation (2016M590804).

Acknowledgment

We thank Dr. Tao Fu for useful discussions.

147.188.108.168 {ts '2017-01-13 09:36:17'}